ACS Chemical Neuroscience

Research Article

pubs.acs.org/chemneuro

Cross-Seeding Interaction between β-Amyloid and Human Islet Amyloid Polypeptide

Rundong Hu,[†,§] Mingzhen Zhang,[†,§] Hong Chen,[†] Binbo Jiang,[†,‡] and Jie Zheng*[,†]

[†]Department of Chemical and Biomolecular Engineering, The University of Akron, Akron, Ohio 44325, United States

[‡]College of Chemical and Biological Engineering, Zhejiang University, Hangzhou, Zhejiang 310027, China

ABSTRACT: Alzheimer's disease (AD) and type 2 diabetes (T2D) are two common protein misfolding diseases. Increasing evidence suggests that these two diseases may be correlated with each other via cross-sequence interactions between β-amyloid peptide (Aβ) associated with AD and human islet amyloid polypeptide (hIAPP) associated with T2D. However, little is known about how these two peptides work and how they interact with each other to induce amyloidogenesis. In this work, we study the effect of cross-sequence interactions between Aβ and hIAPP peptides on hybrid amyloid structures, conformational changes, and aggregation kinetics using combined experimental and simulation approaches. Experimental results confirm that Aβ and hIAPP can interact with each other to aggregate into hybrid amyloid fibrils containing β-sheet-rich structures morphologically similar to pure Aβ and hIAPP. The cross-seeding of Aβ and hIAPP leads to the coexistence of both a retarded process at the initial nucleation stage and an accelerated process at the fibrillization stage, in conjunction with a conformational transition from random structures to α-helix to β-sheet. Further molecular dynamics simulations reveal that Aβ and hIAPP oligomers can efficiently cross-seed each other via the association of two highly similar U-shaped β-sheet structures; thus, conformational compatibility between Aβ and hIAPP aggregates appears to play a key role in determining barriers to cross-seeding. The cross-seeding effects in this work may provide new insights into the molecular mechanisms of interactions between AD and T2D.

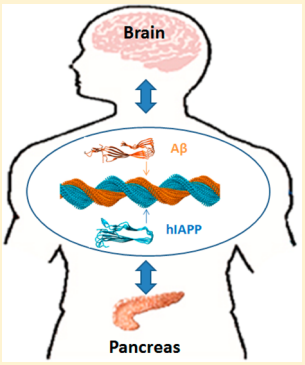

KEYWORDS: *Aβ, hIAPP, amyloid aggregation, cross-seeding, protein misfolding*

A remarkable variety of aged-related neurodegenerative diseases are characterized by the misfolding and aggregation of specific proteins/peptides into amyloid aggregates found in different human tissues.[1] Among more than 20 neurodegenerative diseases, Alzheimer's disease (AD) and type 2 diabetes (T2D) are two common age-related chronic disorders,[2,3] both of which have affected millions of people globally. Emerging evidence from clinical and epidemiological studies has shown a link between AD and T2D.[4,5] It is reported that ∼81% of AD patients are affected by T2D or glucose-related disorders, and AD patients also show a higher risk of developing islet amyloidosis than aged people who are healthy.[6] Meanwhile, T2D patients display cerebral hypometabolism, particularly in brain regions that are characteristically severely affected by AD.[7,8] Although the precise mechanisms linking these two disorders still remain unclear, brain atrophy, reduced cerebral glucose metabolism, and CNS insulin resistance are features of both AD and T2D.

From a different point of view, namely, that abnormal assembly is a common feature of all amyloid proteins and peptides, the AD−T2D link could arise from cross-sequence interactions between the specific, causative peptides associated with the two disorders. In AD, the amyloid-β protein (Aβ, 40−42 amino acids) is a normal cleavage product of the amyloid precursor protein (APP),[9] and Aβ aggregation into senile plaques is a pathological hallmark of AD.[10,11] In T2D, human islet amyloid polypeptide (hIAPP or amylin, a 37-residue hormone peptide) is synthesized in islet β-cells and co-secreted with insulin,[12] and hIAPP polymerizes into amyloid filaments that are associated with the dysfunction and death of islet β-cells.[13,14] Although Aβ and hIAPP have different physiological roles in AD and T2D, under disease conditions both peptides can misfold and aggregate into structurally and functionally similar strains. These strains adopt characteristic cross-β-sheet structures via nucleation−polymerization growth pathways, and they are also highly toxic to surrounding cells and tissues linked to AD or T2D.[15,16] It is generally believed that, prior to the formation of mature amyloid fibrils, numerous small oligomeric assemblies, also known as oligomeric aggregates, are formed at the early stage of nucleation. These oligomeric aggregates have highly polymorphic structures with different sizes, conformations, and morphologies, and some of them contain a certain degree of β-sheet structure.[17] Strong evidence has shown that these soluble oligomeric aggregates are much more toxic to cells than mature fibrils, and they can attack cells in a variety of ways to cause cell dysfunction and even death.[18,19] For example, amyloid oligomers are capable of binding to the cellular membrane to form small channel-like pores,[20] to induce excessive curvature of the membrane,[21] to interfere with the function of membrane-bound receptors, and/or to generate

Received: July 13, 2015
Revised: August 9, 2015
Published: August 10, 2015

DOI: 10.1021/acschemneuro.5b00192
ACS Chem. Neurosci. 2015, 6, 1759−1768

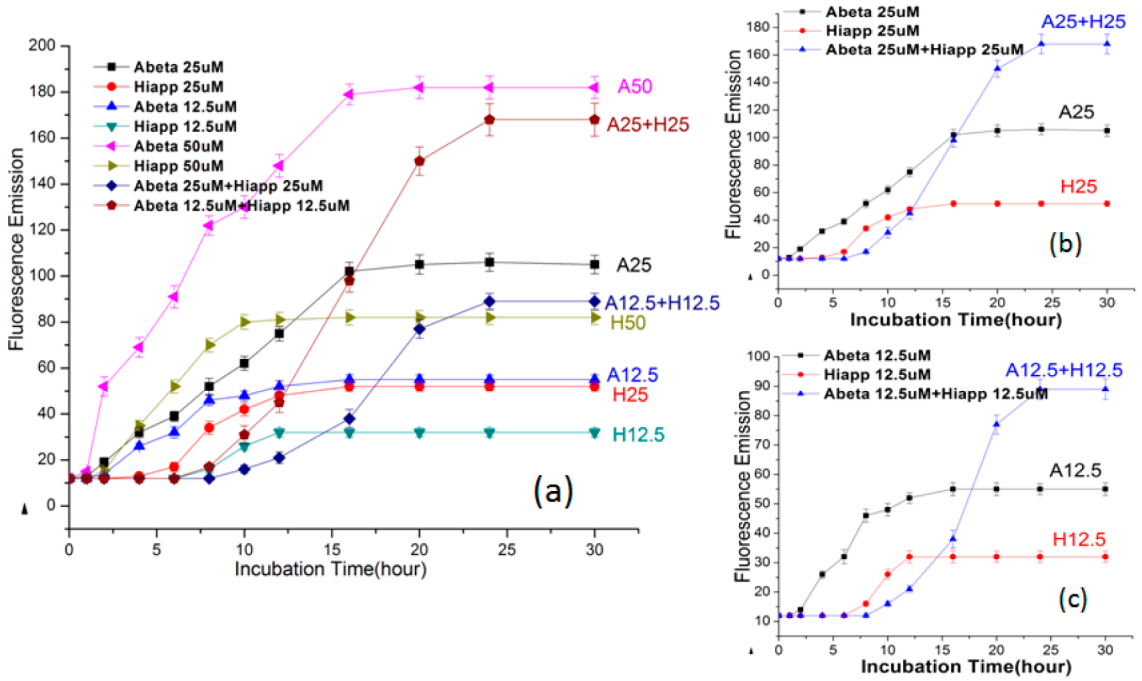

Figure 1. Time-dependent ThT fluorescence curves for pure Aβ, pure hIAPP, and mixed Aβ−hIAPP at different concentration of 12.5, 25, and 50 μM. Error bars represent the average of three replicate experiments.

inflammation. Such oligomer−membrane interactions will cause the disruption of plasma and organelle membranes.[22] Additionally, hIAPP and Aβ show high degrees of sequence identify (25%) and similarity (50%); in particular, these identical and similar sequences are located mainly at the β-strand-forming region.[23,24] More importantly, it has been reported that both Aβ and hIAPP are found in blood serum and cerebrospinal fluid at comparable subnanomolar concentrations. This suggests the possibility that *in vivo* cross-seeding between Aβ and hIAPP could occur to form heterogeneous Aβ−hIAPP aggregates, which travel between cells in the cerebrospinal fluid to induce the neurodegenerative process. Actually, in a broader view, similar cross-seeding behavior between dissimilar amyloid sequences (e.g., Aβ and α-synuclein,[25] Aβ and tau,[26] and hIAPP and insulin[27]) and even between bacterial curli and amyloid peptides of SEVI, Aβ, and hIAPP has been observed.[28] Although the mechanistic models of the cross-seeding between different amyloid peptides are still unclear,[29−32] the evidence for amyloid cross-seeding provides a backdrop for revealing some general principles governing heterogeneous protein misfolding and aggregation. More importantly, the cytotoxicity of amyloid, including Aβ and hIAPP, has been definitively linked to its aggregation; thus, it is likely that the cross-seeding species of Aβ−hIAPP may also possess some cytotoxicity. Regardless of the exact link between AD and T2D, it is equally important to develop effective compounds to suppress the formation of the toxic cross-seeding amyloids. For instance, Vivekanandan et al.[33] used NMR to determine a high-resolution structure of Aβ in aqueous solution. With 3D high-resolution structures of both Aβ and hIAPP available, it becomes more desirable to design compounds to inhibit Aβ or hIAPP aggregation at the early stages of this process, possibly at the monomeric level, because oligomers are known to be neurotoxic.

Several studies have shown that Aβ and hIAPP may cross-seed fibrillization, but they do so with different cross-seeding efficiencies, depending on the experimental conditions (seeding concentrations, sequence specifity, even agitation). O'Nuallain et al.[34] first reported that Aβ fibrils were able to serve as very efficient seeds to interact with hIAPP and thus promote hIAPP aggregation, but hIAPP fibrils were very poor seeds for Aβ aggregation. Later, Yan et al.[35] studied the aggregation kinetics of amyloid fibrils formed by pure Aβ_{40}, pure hIAPP, and mixtures of both peptides at a molar ratio of 1:1. They found that both nucleation and fibrillization of Aβ−hIAPP mixtures were delayed as compared to the aggregation kinetics of pure Aβ or pure hIAPP. They suggest that the cross-seeding of Aβ and hIAPP mixtures was less efficient than homologous seeding of pure Aβ or hIAPP, but such cross-seeding does not necessarily prevent either Aβ or hIAPP aggregation. The following study by the same group[23] confirmed that cross-seeding of Aβ−hIAPP and homoseeding of Aβ and hIAPP likely occur in a competitive manner. In contrast to the cross-seeding of Aβ and hIAPP in the bulk phase, Seeliger et al.[36] investigated the homo- and heteroaggregation processes of Aβ_{40}, hIAPP, and their 1:1 mixture at lipid membranes, with a particular focus on the aggregation of these peptides mediated by effects from the membrane. Interestingly, they found that the mixture of Aβ−hIAPP can aggregate into β-sheet-rich fibrils, whose structures were similar to the structures of pure hIAPP aggregates but different from those of pure Aβ aggregates. Moreover, the aggregation kinetics of Aβ−hIAPP mixtures was slower than that of pure hIAPP, but it was faster than that of Aβ. No cross-inhibition of the fibrillation process in the presence of lipid membrane was observed, and this behavior is similar to the one observed in the bulk.[35] The differential seeding abilities of Aβ vs hIAPP aggregates suggest the existence of different cross-species barriers for different amyloid species to interact with each other and form hybrid amyloids.[37]

Given the current state of knowledge of the cross-seeding of amyloid peptides, it still remains unclear how Aβ and hIAPP interact with each other to induce cross-seeding behavior.

DOI: 10.1021/acschemneuro.5b00192
ACS Chem. Neurosci. 2015, 6, 1759−1768

Herein, we examined the effect of cross-sequence interactions between full-length $A\beta_{1-42}$ and $hIAPP_{1-37}$ on hybrid amyloid structures and aggregation kinetics using combined computational and experimental approaches. We also examined the effect of the concentration of Aβ and hIAPP (12.5−50 μM) on the heteroassembly of Aβ and hIAPP, as well as the cross-seeding efficiency of Aβ−hIAPP in comparison with the homoseeding efficiencies of pure Aβ and hIAPP. The fluorescent dye thioflavin-T (ThT) was used to probe the aggregation kinetics of pure Aβ, pure hIAPP, and Aβ−hIAPP mixtures, and the corresponding fibril morphologies were monitored by atomic force microscopy (AFM). Circular dichroism (CD) spectroscopy was used to record the secondary structure transformation of each peptide group. In parallel, we also computationally modeled and simulated a series of cross-seeding heteroassemblies formed by Aβ and hIAPP peptides using all-atom molecular dynamics (MD) simulations. MD simulations revealed the structural and energetic details of cross-interaction between Aβ and hIAPP peptides at the atomic level. Collective experimental and computational results confirmed the cross-seeding of Aβ and hIAPP, which may provide a different angle to explain the link between AD and T2D. Finally, the mechanisms underlying cross-seeding are discussed. In contrast to the previous work on the cross-seeding of $A\beta_{40}$ and $hIAPP_{37}$ described above, $A\beta_{42}$ is more toxic and amyloidogenic than $A\beta_{40}$ during amyloid aggregation.[38,39] This work hopefully provides some clues to develop strategies that will help to prevent the interaction of Aβ and hIAPP and block a possible link between AD and T2D.

RESULTS AND DISCUSSION

Aggregation Kinetics of Homo- and Heteroaggregation of Aβ and hIAPP. To probe the interaction between Aβ and hIAPP, we first examined and compared the homo- and heteroaggregation processes of Aβ and hIAPP using a ThT fluorescence assay. Figure 1 summarizes the aggregation kinetics of amyloid fibrillation at different molar concentrations of Aβ, hIAPP, and Aβ−hIAPP from 12.5 to 50 μM. To more clearly reveal the cross-seeding effect, Figure 1b,c shows a side-by-side comparison of the ThT curves of two specific groups: one group contains three ThT curves of pure Aβ (25 μM), pure hIAPP (25 μM), and equimolar Aβ−hIAPP mixture (25/25 μM), and the other contains three curves derived from 12.5 μM data. In Figure 1b, when incubating 25 μM Aβ alone at 37 °C for 30 h, the ThT profile showed typical nucleation−polymerization kinetics of amyloid fibrillation, including a 1 h lag phase (nuclei formation) followed by an exponential growth phase (protofibril formation) between 1 and 16 h and a steady phase where mature fibrils were formed after 16 h, as indicated by a final ThT plateau of ∼105. For pure hIAPP, which is not as amyloidogenic as Aβ, it showed a similar, but much slower, nucleation−polymerization kinetics process, with a longer lag phase of 4 h and a much lower plateau of ∼52.

Interestingly, when incubating equimolar Aβ (25 μM) and hIAPP (25 μM) together, the ThT curve displayed a ∼6 h lag phase, which is more slow than that of Aβ and hIAPP alone. This fact at least indicates that Aβ and hIAPP appear to be less prone to aggregate at the early stage of nucleation. This is probably due to the Aβ and hIAPP peptides still being in disordered conformations at the early stage of aggregation, which cannot provide a catalytic surface for homo- or cross-nucleation of either Aβ or hIAPP. Instead, the presence of heterogeneous species seems to interfere with the conformational change and aggregation of the other species, leading to a longer lag phase. However, at the later stages of Aβ−hIAPP aggregation, the aggregation process was accelerated, as indicated by a deeper slope at the growth phase. Finally, the ThT signal achieved a maximum intensity of ∼168 (the maximum ThT intensity is used to quantify the total formation of amyloid fibrils), which was 18% higher than the summation of the maximal ThT intensities of pure Aβ (∼105) and hIAPP (∼52). These maximum ThT results indicate that the coincubation of Aβ and hIAPP indeed leads to the formation of more hybrid amyloid fibrils. Similarly, we performed an additional cross-seeding test of Aβ and hIAPP coincubated at a lower equimolar concentration, 12.5 μM, in comparison with Aβ and hIAPP aggregation alone at 12.5 μM each (Figure 1c). The time of the nucleation phase for the Aβ−hIAPP mixture was 8 h, which was longer than the 1.5 h for Aβ and 6 h for hIAPP. Upon fibrilization, the Aβ−hIAPP mixture produced 20% more amyloid fibrils than their respective contributions from Aβ and hIAPP combined.

From another point of view, when comparing cross-seeding and homoseeding at a total of the same peptide concentrations, it can be seen in Figure 1a that there were clear differences for the maximum ThT intensities between the cross- and homoseeding groups. Specifically, under the same peptide concentrations (in the case of either 25 or 50 μM), the maximum ThT intensities of Aβ−hIAPP were lower than those of pure Aβ, but they were higher than those of pure hIAPP, i.e., the cross-seeding of Aβ−hIAPP is less efficient than the homoseeding of Aβ, but it is more efficient than the homoseeding of hIAPP. So, the Aβ−hIAPP mixture produced less amyloid fibrils than pure Aβ but more fibrils than pure hIAPP. This finding suggests a differential seeding ability between the same and different peptides. The barriers to cross-seeding apparently still exist and depend on the structural compatibility between conformations of two coexisting sequences in the ensemble.

Overall, the fibrillation kinetics monitored by ThT fluorescence reveals an opposite trend for the cross-seeding effect, i.e., retarding aggregation at the initial stage of nucleation but accelerating aggregation at the final stage of fibrillation. During the initial nucleation process, both Aβ and hIAPP peptides exist mainly as monomers and small oligomers, of which most are structurally disordered and dynamically unstable. Such structural diversity and instability (i.e., structural incompatibility) between and within both aggregates create higher cross-species barriers to their interacting with each other, leading to difficulty in cross-seeding each other and thus lengthening the lag phase. Once homoseeds of either Aβ or hIAPP are formed, these seeds may have highly similar structures and consequently can act as templates to efficiently cross-seed each other. Additionally, both homogeneous seeding and heterogeneous seeding coexist in a competitive way.

Conformation Characterization of Cross-Seeding of Aβ and hIAPP. To gain insight into the effect of cross-seeding on the conformational transition of Aβ−hIAPP upon aggregation,[40−42] far-UV CD spectroscopy was applied to monitor changes in the secondary structures for both cross-seeding and homoseeding peptides. All CD samples from different time points were prepared under the same conditions as those for the corresponding ThT samples. As a control, changes in the secondary structure of Aβ and hIAPP were recorded by time-lapse CD spectra over a 24 h period, which

DOI: 10.1021/acschemneuro.5b00192
ACS Chem. Neurosci. 2015, 6, 1759−1768

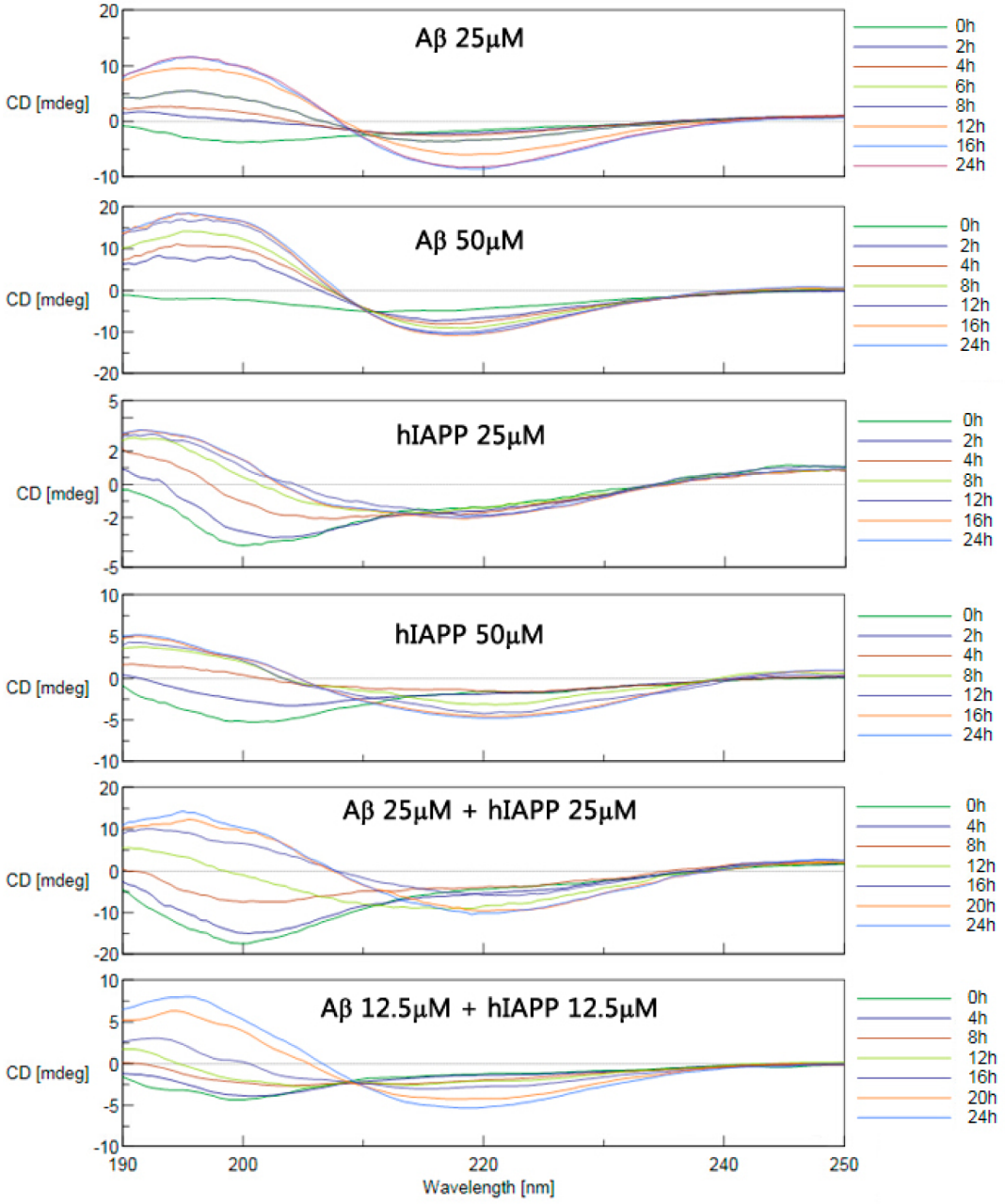

Figure 2. Time-dependent far-UV CD spectra for (a) pure Aβ (25 μM), (b) pure Aβ (50 μM), (c) pure hIAPP (25 μM), (d) pure hIAPP (50 μM), (e) mixed Aβ–hIAPP (25/25 μM), and (f) mixed Aβ–hIAPP (12.5/12.5 μM).

encompasses all of the aggregation states from freshly prepared peptide monomers to mature fibrils.

For homoseeding of Aβ_{42} at 25 μM, the freshly prepared Aβ_{42} initially adopts a random coil conformation with a representative negative minimum of ~197 nm (Figure 2a). Upon protein aggregation for 2 h, this peak diminished gradually, and a positive peak and a negative valley appeared at around 192 and 210 nm, respectively. This indicates that Aβ_{42} converted from its initial random coil to both α-helix and β-sheet structures, consistent with previous studies. Over the next few hours, the positive peak was gradually enhanced and shifted to 195 nm, producing a spectrum dominated by β-sheet, whereas the negative peak kept broadening and deepening, with a minimum ~220 that came from the contribution of both α-helix and β-sheet conformations. At 16–24 h, the CD spectrum stayed almost unchanged and presented a dominant β-sheet conformation accompanied by a certain amount of α-helix. In Figure 2b, homoseeding of Aβ_{42} at 50 μM led to similar changes and shapes in the CD spectra as those of Aβ_{42} at 25 μM, but the higher concentration of Aβ_{42} led to a faster structural transition, as expected. On the basis of the entire CD spectrum, we performed CDpro analysis to obtain the final secondary structure content of Aβ using the CDSSTR method[43] (Figure 3). It can be seen that pure Aβ aggregation at both concentrations gave rise to almost the same secondary structure populations: ~ 30% α-helix and ~50% β-sheet. In Figure 2c,d, pure hIAPP incubated at 25 and 50 μM experienced a similar structural transition: from initial random coils to a combination of α-helix (which was the majority) and β-sheet conformations. The secondary structure distributions of

DOI: 10.1021/acschemneuro.5b00192
ACS Chem. Neurosci. 2015, 6, 1759–1768

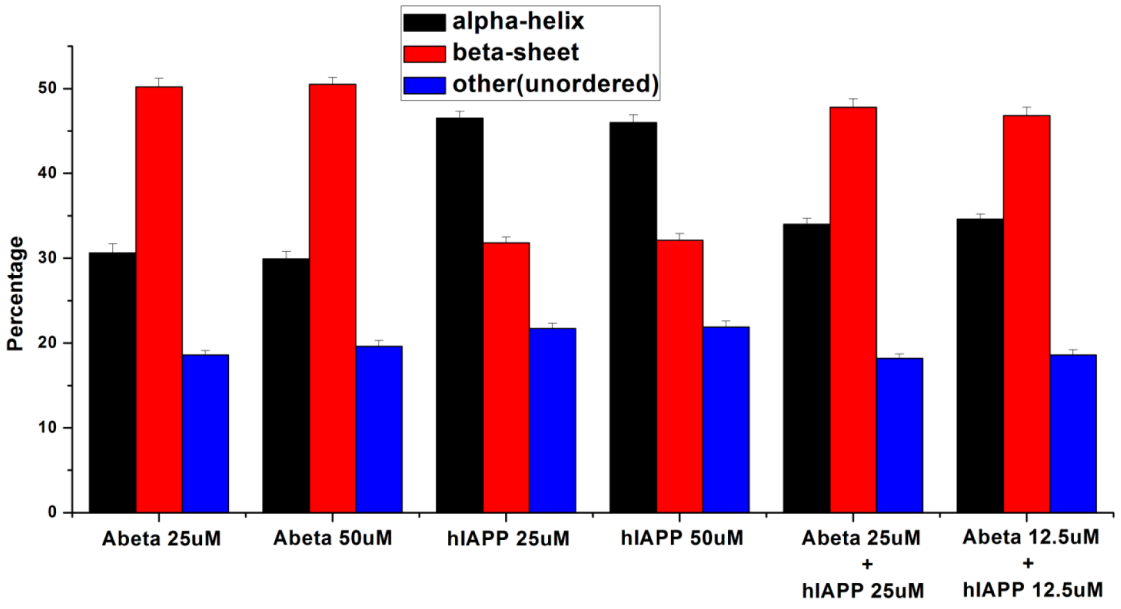

Figure 3. Secondary structure distributions of pure Aβ, pure hIAPP, and mixed Aβ–hIAPP at different concentrations. Error bars represent the average of three replicate experiments.

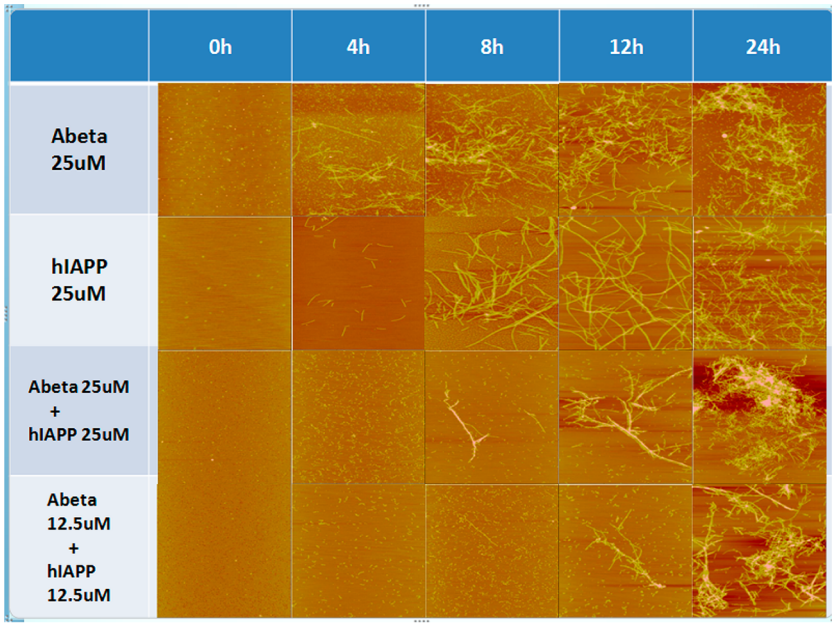

Figure 4. Representative AFM images of pure hIAPP, pure rIAPP, and mixed hIAPP/rIAPP aggregates after incubation for 0, 4, 8, 12, and 24 h.

pure hIAPP were different from those of pure Aβ. hIAPP aggregation led to a higher content of α-helix (~46%) and a lower content of β-sheet (~31%) than those of Aβ (Figure 3).

To examine the effect of cross-seeding on the changes in secondary structure, we recorded CD spectra for Aβ–hIAPP mixture samples, with each species at concentrations of 12.5 and 25 μM. In Figure 2e–f, in the first 8 h of the mixed peptides incubation, the spectra displayed a single negative peak at ~200 nm indicative of a random coil conformation. At 12 h, an α-helix conformation started to appear, at 16 h, α-helix dominated, and at 24 h,the spectra showed a strong positive peak at 195 nm and a negative peak around 220 nm corresponding to a signature for a predominantly β-sheet structure, resembling that of pure Aβ samples. The cross-seeding of Aβ–hIAPP resulted in ~34% α-helix and 47% β-sheet, both of which are similar to those of pure Aβ. In line with the secondary structure data for pure hIAPP, this suggests that the increase in β-sheet content in Aβ–hIAPP comes at the expense of the conversion of the α-helix of hIAPP to the β-sheet. Overall, the CD data obtained from the cross-seeding of Aβ–hIAPP present a continuous decline in random structure, a transient rise in α-helix content, and a gradual increase in β-sheet content, consistent with the ThT data that indicates cross-sequence interactions between Aβ and hIAPP.

Structural Morphologies of Homoseeding and Cross-Seeding Amyloid Fibrils. Another way to monitor the kinetics of fibril formation is to follow structural changes using AFM. Figure 4 shows a series of topographical AFM images of Aβ, hIAPP, and Aβ–hIAPP samples deposited on mica surfaces as a function of incubation time at 37 °C. All of the AFM

DOI: 10.1021/acschemneuro.5b00192
ACS Chem. Neurosci. 2015, 6, 1759–1768

samples prepared at different time points were collected under the same conditions as the ones used for the ThT and CD experiments. Overall, it is confirmed that all homoseeding and cross-seeding samples formed fibrils at 24 h and that the morphologies of the mature fibrils were similar in all cases. However, homoseeding and cross-seeding showed different fibril formation kinetics. As a control, hIAPP (25 μM) alone showed no amyloid or amorphous aggregates at 0 h. After 4 h, a few dispersed spherical particles with diameters of 1−2 nm were observed. After that, some protofibrils with an average height of 7−8 nm continued to grow into the thicker and longer mature fibrils with average heights of 10−12 nm. Compared to hIAPP, Aβ (25 μM) had a faster rate of aggregation for forming mature fibrils at the expense of monomers and small amorphous aggregates. As compared to homoseeding of Aβ or hIAPP, Aβ−hIAPP samples (25/25 μM) showed a longer lag process, during which many amorphous aggregates and a few wormlike protofibrils were formed at 8 h. The prolonged lag phase became even more pronounced for the lower concentration Aβ−hIAPP samples (12.5/12.5 μM). However, at 24 h, all Aβ−hIAPP mixtures were able to form morphologically similar amyloids to those of pure Aβ or hIAPP amyloids. The AFM results were generally in line with the earlier fibril formation findings by ThT and CD. Collectively, the data confirm that the species barriers initially decelerate the nucleation stage, during which most amyloid aggregates adopt random structures, and that such structural incompatibility between amyloid aggregates of the same and different sequences may induce steric hindrance and thus prevent nucleus formation. Once the critical nuclei are formed, cross-seeding interactions between Aβ and hIAPP become possible, and the coexistence of Aβ and hIAPP enhances the transition from α-helix to β-sheet. Both effects promote the fibrillation process.

MD Simulations of Cross-Sequence Interactions between Aβ and hIAPP. To reveal atomic details of the cross-sequence interactions between Aβ and hIAPP, we computationally modeled and simulated a series of cross-seeding assemblies formed by Aβ and hIAPP peptides using a peptide-packing program developed in our previous work.[44,45] A number of computational studies have shown that Aβ and hIAPP pentamers exhibit high structural stability with well-preserved U-bend (β-strand−turn−β-strand) β-structures;[46−48] thus, Aβ and hIAPP pentamers were selected as the basic building units to study cross-seeding interactions between them in a lateral association manner, i.e., Aβ and hIAPP oligomers were stacked on top of each other to form double-layer assemblies. A recent computational study by Berhanu et al.[49] has shown that both Aβ and hIAPP oligomers can cross-seed each other in an elongation manner; thus, we will not discuss the elongation models here. Among 1080 Aβ−hIAPP double-layer assemblies being generated, two Aβ−hIAPP assemblies ($_a$CN$_h$ and $_a$NN$_h$) were prominent with respect to the other assemblies, as supported by their higher structural population, lower conformational energy, and better structural stability. As shown in Figure 5, for the $_a$CN$_h$ Aβ−hIAPP assembly, Aβ and hIAPP pentamers associated together in parallel fashion and formed a hybrid interface via the C-terminal β-sheet of Aβ and N-terminal β-sheet of hIAPP. Differently, the $_a$NN$_h$ assembly adopted antiparallel packing between the Aβ and hIAPP pentamers and formed a NN interface by the N-terminal β-sheet of Aβ and N-terminal β-sheet of hIAPP. To monitor the layer-to-layer association of Aβ−hIAPP assemblies, Figure 6a,b shows the interlayer distances between the backbone residues of two facing β-sheets associated through (a) the CN interface (i.e., Aβ^{42}−hIAPP^{11}, Aβ^{39}−hIAPP^{15}, and Aβ^{35}−hIAPP^{17}) and (b) the NN interface (i.e., Aβ^{24}−hIAPP^{11} and Aβ^{20}−hIAPP^{15}). It can be seen clearly that, within the 80 ns MD simulations, both $_a$CN$_h$ and $_a$NN$_h$ assemblies retained a steady layer-to-layer distance of 6.5 Å for $_a$CN$_h$ and 7.1 Å for $_a$NN$_h$, so no disassociation between Aβ and hIAPP pentamers was observed for both assemblies. The relatively constant interlayer distances also indicate that Aβ and hIAPP have fairly good backbone and side chain interactions with each other. Consistently, both assemblies also displayed high structural stability, as evidenced by the small and steady RMSD values of ∼4.5 Å for both $_a$CN$_h$ and $_a$NN$_h$ assemblies. As a result, both assemblies can well retain their original U-shaped β-sheet structures, with a dominant β-sheet content of ∼50% for Aβ and hIAPP in both assemblies (Figure 6c).

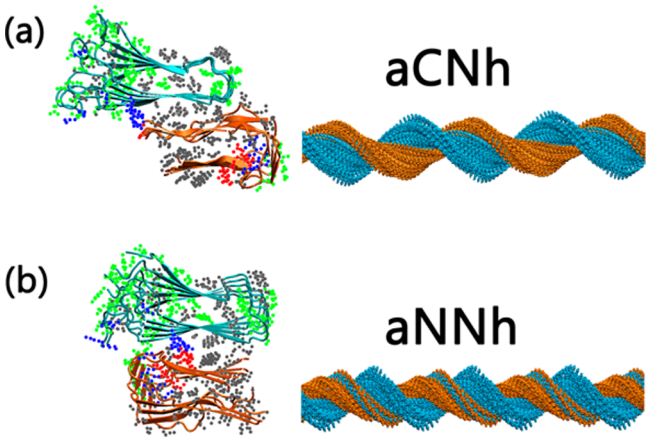

Figure 5. Cross-sectional oligomeric structure and fibrillar structure of Aβ(orange)/hIAPP(cyan) for (a) $_a$CN$_h$ and (b) $_a$NN$_h$ arrangements. Residues are represented by small dots of different colors: polar residues (green dots), nonpolar residues (gray dots), basic residues (blue dots), and acidic residues (red dots).

Both assemblies covered the long interface with a maximum overlap of the two β-sheets between Aβ and hIAPP, forming a well-packed steric zipper interface. However, both assemblies apparently involved different interfacial residues to stabilize their interfaces and whole structures. The $_a$CN$_h$ interface mainly consisted of five residues (A42, I41, V39, G37, M35, and G33) from the Aβ pentamer and another five residues (R11, A13, F15, V17, S19) from the hIAPP pentamer; thus, this interface is mainly governed by hydrophobic contacts and salt bridges. The $_a$NN$_h$ assembly involved hydrophobic interactions among V24, F20, and V18 of Aβ and A13, F15, and V17 of hIAPP, salt bridges between E22 of Aβ and R11 of hIAPP, and π−π stacking between F20 of Aβ and F15 of hIAPP. Despite the diversity of these stabilizing forces, the average interlayer interactions between Aβ and hIAPP were −357.5 ± 7.0 kcal/mol for $_a$CN$_h$ and −315.7 ± 21.9 kcal/mol for $_a$NN$_h$, respectively (Figure 6d), suggesting that $_a$CN$_h$ is more engerentically favorable than $_a$NN$_h$. Decomposition of the total interlayer interaction energy into vdW and electrostatic components further revealed that electrostatic interactions clearly play a dominant role in interlayer interactions, contributing almost 90% to Aβ−hIAPP association in both assemblies. These models suggest that structural similarities can lead to amyloids composed of different sequences.

DOI: 10.1021/acschemneuro.5b00192
ACS Chem. Neurosci. 2015, 6, 1759−1768

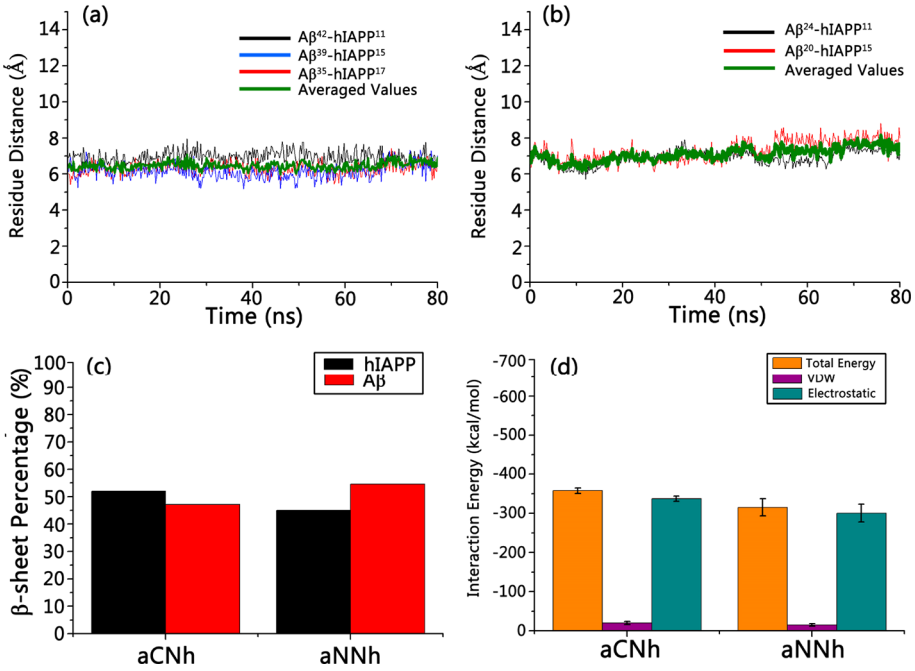

Figure 6. Structural and energetic characteristics of Aβ–hIAPP assemblies. Interlayer distances between backbone residues of two facing β-sheets for (a) ${}_{a}CN_{h}$ and (b) ${}_{a}NN_{h}$ assemblies. The residue–residue distance was defined as the separation between the centers of mass of the selected residues of Aβ and hIAPP. The superscript number denotes the selected residue IDs in Aβ and hIAPP. (c) Average β-sheet percentage of individual Aβ and hIAPP pentamers for each hybrid model. (d) Interlayer interactions and its decomposed energy contributions between Aβ and hIAPP for both Aβ–hIAPP assemblies, calculated by the GBMV method with the CHARMM27 force field.

CONCLUSIONS

Clinical studies report that persons suffering from T2D might be at the risk of AD, and vice versa, suggesting that AD and T2D might be linked to each other. $A\beta_{1-42}$ and $hIAPP_{1-37}$ are the two amyloidogenic peptides that can self-assemble into cytotoxic aggregates and amyloid fibrils associated with AD and T2D, respectively. However, the exact role of cross-seeding between Aβ and hIAPP in the progression of AD and T2D still remains unclear. Herein, we studied the molecular structures, aggregation kinetics, and conformational changes of Aβ and hIAPP cross-seeding using combined experimental and computational approaches. Aβ–hIAPP mixtures at different concentrations indeed showed cross-seeding behavior by forming hybrid amyloid fibrils morphologically similar to pure Aβ or hIAPP fibrils. The cross-seeding of Aβ–hIAPP also led to a retardation of peptide aggregation at the initial stage of nucleation because of the structural incompatibility between different amyloid aggregates, but it accelerated the aggregation at the final stage of fibrillation because of the formation of similar seed structures as templates for promoting cross-seeding. The cross-seeding of Aβ–hIAPP presented a structural conversion from a random structure to a transient α-helix and to a gradual increase in β-sheet content. Cross-seeding effects at different stages of aggregation suggest that structural compatibility between amyloid aggregates of different sequences determines the barriers to cross-seeding. Finally, molecular modeling and MD simulations confirmed that, with 25% sequence identity and 50% sequence similarity, both Aβ and hIAPP oligomers that adopted conformationally similar U-bend structures were able to associate together via ${}_{a}CN_{h}$ and ${}_{a}NN_{h}$ interfaces. Meanwhile, the Aβ–hIAPP heteroassembly models provide possible structures and interaction models to demonstrate the existence of the Aβ–hIAPP cross-seeding species under certain conditions. These Aβ–hIAPP models do not necessarily exclude other structural models due to the complex, polymorphic species of amyloid peptides. This work hopefully provides a molecular explanation for the potential link between AD and T2D and may offer a clue for the design of novel therapeutic compounds and concepts against both of these as-yet incurable amyloid diseases.

METHODS

Regents. 1,1,1,3,3,3-Hexafluoro-2-propanol (HFIP, ≥99.9%), dimethyl sulfoxide (DMSO, ≥99.9%), 10 mM PBS buffer (pH 7.4), 10 mM NaOH, and thioflavin T (ThT, 98%) were purchased from Sigma-Aldrich (St. Louis, MO). Human IAPP (1–37) (≥95.0%) and Aβ(1–42) (≥95.0%) were purchased from American Peptide Inc. (Sunnyvale, CA). All other chemicals were of the highest grade available.

Peptide Purification and Preparation. Both and Aβ and hIAPP peptides were obtained in a lyophilized form and stored at −20 °C. In order to prepare the monomeric peptide solution, 1.0 mg of each preaggregated peptide was dissolved in HFIP for 2 h, sonicated for 30 min to remove any pre-existing aggregates or seeds, and centrifuged at 14 000 rpm for 30 min at 4 °C. 80% of the top peptide solution was then extracted, subpackaged, frozen with liquid nitrogen, and then dried with a freeze-dryer. The dry peptide powder was lyophilized at −80 °C and used within 1 week.

A homogeneous monomer solution of peptide is required for studying amyloid formation. 0.2 mg of purified hIAPP or Aβ powder was aliquoted in 25 μL of a 10 mM NaOH solution and sonicated for 1 min to obtain a homogeneous solution. The initiation of Aβ (25 μM) aggregation in solution was accomplished by adding that 25 μL NaOH–Aβ solution to 2 mL of 10 mM PBS buffer. This solution was then centrifuged at 14 000 rpm for 30 min at 4 °C to remove any existing oligomers, and 80% of the top solution was removed for further incubation. We used the same protocol to prepare hIAPP solutions or mixed Aβ–hIAPP solutions, with the only difference being a change in the initial amount and ratio of purified powder. All solutions were incubated at 37 °C.

DOI: 10.1021/acschemneuro.5b00192
ACS Chem. Neurosci. 2015, 6, 1759–1768

Thioflavin T (ThT) Fluorescence Assay. The ThT fluorescence assay is a standard method to detect the formation of amyloid fibrils because ThT can specifically bind to the β-sheet structure of protein fibrils, resulting in a strong fluorescence emission.[50] A ThT solution (2 mM) was prepared by adding 0.033 g of ThT powder into 50 mL of DI water. The resulting 250 μL of the 2 mM ThT solution was further diluted into 50 mL of Tris-buffer (pH 7.4) to a final concentration of 10 μM. 60 μL of peptide solution was put into 3 mL of 10 μM ThT-Tris solution. Fluorescence spectra were obtained using a LS-55 fluorescence spectrometer (PerkinElmer Corp., Waltham, MA). All measurements were carried out in aqueous solution using a 1 cm × 1 cm quartz cuvette. ThT fluorescence emission wavelengths were recorded between 470 and 500 nm with an excitation wavelength of 450 nm. Each experiment was repeated at least three times, and each sample was tested in quintuplicate.

Circular Dichroism Spectroscopy (CD). The secondary structures of Aβ and hIAPP in solution were examined by CD spectroscopy with a J-1500 spectropolarimeter (Jasco Inc., Japan) using a continuous scanning mode at room temperature. Peptide solutions incubated for 0, 2, 4, 6, 8, 12, 16, and 24 h (160 μL for each time point) were placed into a rectangular quartz cuvette of a 1 mm path length without dilution. The spectra were scanned between 250 and 190 nm at a 0.5 nm resolution and 50 nm/min scan rate. All spectra were corrected by subtracting the baseline and averaged by three successive scans for each sample. The secondary structure content was calculated from the CD spectra using the self-consistent method (CDSSTR program) by CDpro analysis software.[43,51]

Tapping-Mode AFM. Morphology changes of peptides during fibrillization were monitored by a tapping-mode AFM. A 20 μL sample used in the ThT fluorescence assay was taken for AFM measurement at different time points in order to correlate Aβ or hIAPP morphological changes with their growth kinetics. The peptide solution was deposited onto a freshly cleaved mica substrate for 1 min, rinsed three times with 50 mL of DI water to remove salts and loosely bound peptide, and dried with compressed air for 5 min before AFM imaging. Tapping mode AFM imaging was performed in air using a Nanoscope III multimode scanning probe microscope (Veeco Corp., Santa Barbara, CA) equipped with a 15 μm E scanner. Commercial Si cantilevers (NanoScience) with an elastic modulus of 40 N m^{-1} were used. All images were acquired as 512 × 512 pixel images at a typical scan rate of 1.0−2.0 Hz with a vertical tip oscillation frequency of 250−350 kHz.[52] Representative AFM images were obtained by scanning at least six different locations of different samples.

MD Simulation System and Simulation Protocol. The polymorphic morphology of amyloid peptides is thought to be one of the structural characteristics of amyloids. Due to the polymorphic morphology of amyloid peptides, different atomic structural models of hIAPP have been proposed by Tycko's,[13] Eisenberg's,[53] and Miller's laboratories.[54] Although all of these models adopted a similar U-bend β-sheet structure, Miller and co-workers[54] found that even a subtle change in the side chain orientation of hIAPP can lead to different self-assembled hIAPP fibrillar forms. In this work, Aβ and hIAPP pentamers were extracted from the fibrillar structures of Aβ (PDB: 2BEG)[55] and hIAPP from Tycko's lab,[13] respectively. Both pentamers adopt similar β-strand−loop−β-strand (U-bend) fold. To obtain possible stable cross-seeding assemblies of Aβ−hIAPP, we applied an in-house peptide-packing program[45,56−59] to screen all possible layer-to-layer associations between Aβ and hIAPP pentamers by considering the interlayer distance between two pentamers along the y axis (d_y, along lateral direction) and the interlayer translation along the x axis (d_x, one layer was translated with respect to the other along the β-strand direction), where d_x and d_y are the two key parameters for controlling structural stability and packing energy of hybrid Aβ−hIAPP aggregates. This search strategy has been successfully used to predict both homo- and heteroassemblies of Aβ, hIAPP, and hIAPP/rIAPP. Considering that both Aβ and hIAPP pentamers have two respective and distinctive β-sheets (C-terminal β-sheet and N-terminal β-sheet), they can be associated laterally with each other to form different hybrid double-layer structures via four typical interfaces ($_aCC_h$, $_aCN_h$, $_aNC_h$, and $_aNN_h$) and two packing orientations (parallel and antiparallel) between Aβ and hIAPP pentamers. Consequently, a total of 1080 Aβ−hIAPP assemblies were generated; among them, two assemblies of $_aCN_h$ and $_aNN_h$ showed the most stable structures at the lowest energy state and will be used as examples to illustrate the structural aspects of Aβ−hIAPP cross-seedings. The two Aβ−hIAPP assemblies were solvated in a TIP3P water box with a margin of at least 15 Å from any edge of the water box to any peptide atom. Any water molecule within 2.6 Å of the peptide was removed. Each system was then neutralized by the addition of Cl^- and Na^+ ions to mimic ~150 mM ionic strength. Then, the Aβ−hIAPP systems were energy-minimized by 5000 steps of steepest decent minimization. The systems were then gradually heated from 0 to 310 K by 2 ns MD simulations. MD production runs were conducted for 80 ns using the NPT ensemble (T = 310 K and P = 1 atm) under periodic boundary conditions. Short-range van der Waals (VDW) interactions were described by the smoothly truncated method via potential shift at 14 Å. Long-range electrostatic interactions were calculated by the particle mesh Ewald (PME) method with a grid spacing of 0.16 Å and a real-space cutoff of 12 Å. The equations of motion were integrated using the Leapfrog integrator with a time step of 2 fs. All explicit-solvent all-atom simulations were conducted using the Gromacs 4.6.5 program.[60,61]

Generalized Born Method with Molecular Volume (GBMV). To obtain the interaction energy between Aβ and hIAPP for both models, we extracted the model trajectories of the last 10 ns from the explicit-solvent MD simulations by deleting all explicit water molecules and ions. The GBMV implicit solvent model with the CHARMM force field is used for mimicking the Poisson−Boltzmann (PB) electrostatic solvation energy. In the GBMV calculations, the dielectric constant of water was set to 80, whereas the hydrophobic solvent-accessible surface area (SASA) term factor was set to 0.00592 kcal/(mol Å^2). The extracted trajectories were first energy-minimized by 500-step steepest descent minimization, followed by interaction energy calculation by the grid-based GBMV, in which the van der Waals and electrostatic interaction terms for each model were obtained.

AUTHOR INFORMATION

Corresponding Author

*Phone: 330-972-2096; Fax: 330-972-5856; E-mail: zhengj@uakron.edu.

Author Contributions

§R.H. and M.Z. contributed equally to this work.

Author Contributions

R.H., M.Z., and J.Z. designed the research; R.H., M.Z. and H.C. performed the research; R.H., M.Z., B.J., and J.Z. analyzed the data; and R.H., M.Z., and J.Z. wrote the paper.

Funding

We thank the NSF (CAREER Award CBET-0952624 and CBET-1510099) and the Alzheimer's Association (New Investigator Research Grant, 2015-NIRG-341372), for support.

Notes

The authors declare no competing financial interest.

ACKNOWLEDGMENTS

We gratefully thank the Tycko lab for providing NMR structures of hIAPP1-37.

REFERENCES

(1) Chiti, F., and Dobson, C. M. (2006) Protein misfolding, functional amyloid, and human disease. *Annu. Rev. Biochem. 75*, 333−366.

(2) Shankar, G. M., Li, S., Mehta, T. H., Garcia-Munoz, A., Shepardson, N. E., Smith, I., Brett, F. M., Farrell, M. A., Rowan, M. J., Lemere, C. A., Regan, C. M., Walsh, D. M., Sabatini, B. L., and Selkoe, D. J. (2008) Amyloid-[beta] protein dimers isolated directly from

DOI: 10.1021/acschemneuro.5b00192
ACS Chem. Neurosci. 2015, 6, 1759−1768

Alzheimer's brains impair synaptic plasticity and memory. *Nat. Med. 14*, 837−842.
(3) DeToma, A. S., Salamekh, S., Ramamoorthy, A., and Lim, M. H. (2012) Misfolded proteins in Alzheimer's disease and type II diabetes. *Chem. Soc. Rev. 41*, 608−621.
(4) Janson, J., Laedtke, T., Parisi, J. E., O'Brien, P., Petersen, R. C., and Butler, P. C. (2004) Increased risk of type 2 diabetes in Alzheimer disease. *Diabetes 53*, 474−481.
(5) Nicolls, M. R. (2004) The Clinical and Biological Relationship between Type II Diabetes Mellitus and Alzheimers Disease. *Curr. Alzheimer Res. 1*, 47−54.
(6) Jucker, M., and Walker, L. C. (2011) Pathogenic protein seeding in Alzheimer disease and other neurodegenerative disorders. *Ann. Neurol. 70*, 532−540.
(7) Sims-Robinson, C., Kim, B., Rosko, A., and Feldman, E. L. (2010) How does diabetes accelerate Alzheimer disease pathology? *Nat. Rev. Neurol. 6*, 551−559.
(8) Vagelatos, N. T., and Eslick, G. D. (2013) Type 2 diabetes as a risk factor for Alzheimer's disease: the confounders, interactions, and neuropathology associated with this relationship. *Epidemiol. Rev. 35*, 152−160.
(9) Citron, M., Teplow, D. B., and Selkoe, D. J. (1995) Generation of amyloid β protein from its precursor is sequence specific. *Neuron 14*, 661−670.
(10) Hardy, J., and Selkoe, D. J. (2002) The Amyloid Hypothesis of Alzheimer's Disease: Progress and Problems on the Road to Therapeutics. *Science 297*, 353−356.
(11) Williams, T. L., and Serpell, L. C. (2011) Membrane and surface interactions of Alzheimer's Aβ peptide − insights into the mechanism of cytotoxicity. *FEBS J. 278*, 3905−3917.
(12) Cooper, G. J., Day, A. J., Willis, A. C., Roberts, A. N., Reid, K. B., and Leighton, B. (1989) Amylin and the amylin gene: structure, function and relationship to islet amyloid and to diabetes mellitus. *Biochim. Biophys. Acta, Mol. Cell Res. 1014*, 247−258.
(13) Luca, S., Yau, W.-M., Leapman, R., and Tycko, R. (2007) Peptide conformation and supramolecular organization in amylin fibrils: constraints from solid-state NMR. *Biochemistry 46*, 13505−13522.
(14) Brender, J. R., Salamekh, S., and Ramamoorthy, A. (2012) Membrane disruption and early events in the aggregation of the diabetes related peptide IAPP from a molecular perspective. *Acc. Chem. Res. 45*, 454−462.
(15) Eisenberg, D., Nelson, R., Sawaya, M. R., Balbirnie, M., Sambashivan, S., Ivanova, M. I., Madsen, A. O., and Riekel, C. (2006) The structural biology of protein aggregation diseases: fundamental questions and some answers. *Acc. Chem. Res. 39*, 568−575.
(16) Bemporad, F., Calloni, G., Campioni, S., Plakoutsi, G., Taddei, N., and Chiti, F. (2006) Sequence and structural determinants of amyloid fibril formation. *Acc. Chem. Res. 39*, 620−627.
(17) Miller, Y., Ma, B., and Nussinov, R. (2011) Alzheimer Aβ Amyloid Annular Fibrils: Insight Into Polymorphism. *Biophys. J. 100*, 531a.
(18) Brender, J. R., Lee, E. L., Hartman, K., Wong, P. T., Ramamoorthy, A., Steel, D. G., and Gafni, A. (2011) Biphasic effects of insulin on islet amyloid polypeptide membrane disruption. *Biophys. J. 100*, 685−692.
(19) Brender, J. R., Lee, E. L., Cavitt, M. A., Gafni, A., Steel, D. G., and Ramamoorthy, A. (2008) Amyloid fiber formation and membrane disruption are separate processes localized in two distinct regions of IAPP, the type-2-diabetes-related peptide. *J. Am. Chem. Soc. 130*, 6424−6429.
(20) Sciacca, M. F., Kotler, S. A., Brender, J. R., Chen, J., Lee, D.-K., and Ramamoorthy, A. (2012) Two-step mechanism of membrane disruption by abeta through membrane fragmentation and pore formation. *Biophys. J. 103*, 702−710.
(21) Brender, J. R., Salamekh, S., and Ramamoorthy, A. (2012) Membrane disruption and early events in the aggregation of the diabetes related peptide IAPP from a molecular perspective. *Acc. Chem. Res. 45*, 454−462.
(22) Patel, H. R., Pithadia, A. S., Brender, J. R., Fierke, C. A., and Ramamoorthy, A. (2014) In search of aggregation pathways of IAPP and other amyloidogenic proteins: finding answers through NMR spectroscopy. *J. Phys. Chem. Lett. 5*, 1864−1870.
(23) Andreetto, E., Yan, L.-M., Tatarek-Nossol, M., Velkova, A., Frank, R., and Kapurniotu, A. (2010) Identification of hot regions of the Aβ−IAPP interaction interface as high-affinity binding sites in both cross- and self-association. *Angew. Chem., Int. Ed. 49*, 3081−3085.
(24) Lu, Y., Derreumaux, P., Guo, Z., Mousseau, N., and Wei, G. (2009) Thermodynamics and dynamics of amyloid peptide oligomerization are sequence dependent. *Proteins: Struct., Funct., Genet. 75*, 954−963.
(25) Mandal, P. K., Pettegrew, J. W., Masliah, E., Hamilton, R. L., and Mandal, R. (2006) Interaction between Aβ peptide and α synuclein: molecular mechanisms in overlapping pathology of Alzheimer's and Parkinson's in dementia with Lewy body disease. *Neurochem. Res. 31*, 1153−1162.
(26) Stancu, I.-C., Vasconcelos, B., Terwel, D., and Dewachter, I. (2014) Models of β-amyloid induced Tau-pathology: the long and "folded" road to understand the mechanism. *Mol. Neurodegener. 9*, 51.
(27) Liu, P., Zhang, S., Chen, M.-s., Liu, Q., Wang, C., Wang, C., Li, Y.-M., Besenbacher, F., and Dong, M. (2012) Co-assembly of human islet amyloid polypeptide (hIAPP)/insulin. *Chem. Commun. 48*, 191−193.
(28) Hartman, K., Brender, J. R., Monde, K., Ono, A., Evans, M. L., Popovych, N., Chapman, M. R., and Ramamoorthy, A. (2013) Bacterial curli protein promotes the conversion of PAP248−286 into the amyloid SEVI: cross-seeding of dissimilar amyloid sequences. *PeerJ 1*, e5.
(29) Morales, R., Moreno-Gonzalez, I., and Soto, C. (2013) Cross-seeding of misfolded proteins: implications for etiology and pathogenesis of protein misfolding diseases. *PLoS Pathog. 9*, e1003537.
(30) Morales, R., Estrada, L. D., Diaz-Espinoza, R., Morales-Scheihing, D., Jara, M. C., Castilla, J., and Soto, C. (2010) Molecular cross talk between misfolded proteins in animal models of Alzheimer's and prion diseases. *J. Neurosci. 30*, 4528−4535.
(31) Guo, J.-P., Arai, T., Miklossy, J., and McGeer, P. L. (2006) Aβ and tau form soluble complexes that may promote self aggregation of both into the insoluble forms observed in Alzheimer's disease. *Proc. Natl. Acad. Sci. U. S. A. 103*, 1953−1958.
(32) Morales, R., Green, K. M., and Soto, C. (2009) Cross currents in protein misfolding disorders: interactions and therapy. *CNS Neurol. Disord.: Drug Targets 8*, 363.
(33) Vivekanandan, S., Brender, J. R., Lee, S. Y., and Ramamoorthy, A. (2011) A partially folded structure of amyloid-beta(1−40) in an aqueous environment. *Biochem. Biophys. Res. Commun. 411*, 312−316.
(34) O'Nuallain, B., Williams, A. D., Westermark, P., and Wetzel, R. (2004) Seeding specificity in amyloid growth induced by heterologous fibrils. *J. Biol. Chem. 279*, 17490−17499.
(35) Yan, L. M., Velkova, A., Tatarek - Nossol, M., Andreetto, E., and Kapurniotu, A. (2007) IAPP Mimic Blocks Aβ Cytotoxic Self - Assembly: Cross - Suppression of Amyloid Toxicity of Aβ and IAPP Suggests a Molecular Link between Alzheimer's Disease and Type II Diabetes. *Angew. Chem., Int. Ed. 46*, 1246−1252.
(36) Seeliger, J., Evers, F., Jeworrek, C., Kapoor, S., Weise, K., Andreetto, E., Tolan, M., Kapurniotu, A., and Winter, R. (2012) Cross - Amyloid Interaction of Aβ and IAPP at Lipid Membranes. *Angew. Chem., Int. Ed. 51*, 679−683.
(37) Ma, B., and Nussinov, R. (2012) Selective molecular recognition in amyloid growth and transmission and cross-species barriers. *J. Mol. Biol. 421*, 172−184.
(38) Jan, A., Gokce, O., Luthi-Carter, R., and Lashuel, H. A. (2008) The ratio of monomeric to aggregated forms of Aβ40 and Aβ42 is an important determinant of amyloid-β aggregation, fibrillogenesis, and toxicity. *J. Biol. Chem. 283*, 28176−28189.
(39) Bitan, G., Kirkitadze, M. D., Lomakin, A., Vollers, S. S., Benedek, G. B., and Teplow, D. B. (2003) Amyloid β-protein (Aβ) assembly: Aβ40 and Aβ42 oligomerize through distinct pathways. *Proc. Natl. Acad. Sci. U. S. A. 100*, 330−335.

DOI: 10.1021/acschemneuro.5b00192
ACS Chem. Neurosci. 2015, 6, 1759−1768

(40) Johnson, W. C. (1990) Protein secondary structure and circular dichroism: a practical guide. *Proteins: Struct., Funct., Genet. 7*, 205−214.
(41) Greenfield, N. J. (2007) Using circular dichroism spectra to estimate protein secondary structure. *Nat. Protoc. 1*, 2876−2890.
(42) Calloni, G., Lendel, C., Campioni, S., Giannini, S., Gliozzi, A., Relini, A., Vendruscolo, M., Dobson, C. M., Salvatella, X., and Chiti, F. (2008) Structure and dynamics of a partially folded protein are decoupled from its mechanism of aggregation. *J. Am. Chem. Soc. 130*, 13040−13050.
(43) Sreerama, N., and Woody, R. W. (2000) Estimation of protein secondary structure from circular dichroism spectra: comparison of CONTIN, SELCON, and CDSSTR methods with an expanded reference set. *Anal. Biochem. 287*, 252−260.
(44) Zhao, J., Yu, X., Liang, G., and Zheng, J. (2011) Structural polymorphism of human islet amyloid polypeptide (hIAPP) oligomers highlights the importance of interfacial residue interactions. *Biomacromolecules 12*, 210−220.
(45) Zhang, M., Hu, R., Chen, H., Chang, Y., Gong, X., Liu, F., and Zheng, J. (2015) Interfacial interaction and lateral association of cross-seeding assemblies between hIAPP and rIAPP oligomers. *Phys. Chem. Chem. Phys. 17*, 10373−10382.
(46) Liang, G., Zhao, J., Yu, X., and Zheng, J. (2013) Comparative molecular dynamics study of human islet amyloid polypeptide (IAPP) and rat IAPP oligomers. *Biochemistry 52*, 1089−1100.
(47) Zheng, J., Jang, H., Ma, B., Tsai, C.-J., and Nussinov, R. (2007) Modeling the alzheimer a{beta}17−42 fibril architecture: tight intermolecular sheet-sheet association and intramolecular hydrated cavities. *Biophys. J. 93*, 3046−3057.
(48) Zheng, J., Ma, B., Chang, Y., and Nussinov, R. (2008) Molecular dynamics simulations of alzheimer's peptide A[beta]40 elongation and lateral association. *Front. Biosci., Landmark Ed. 13*, 3919−3930.
(49) Berhanu, W. M., Yaşar, F., and Hansmann, U. H. E. (2013) In silico cross seeding of Aβ and amylin fibril-like oligomers. *ACS Chem. Neurosci. 4*, 1488−1500.
(50) Biancalana, M., and Koide, S. (2010) Molecular mechanism of Thioflavin-T binding to amyloid fibrils. *Biochim. Biophys. Acta, Proteins Proteomics 1804*, 1405−1412.
(51) Juszczyk, P., Kolodziejczyk, A., and Grzonka, Z. (2005) Circular dichroism and aggregation studies of amyloid beta (11−28) fragment and its variants. *Acta Biochim. Pol. 52*, 425−431.
(52) Wang, Q., Yu, X., Patal, K., Hu, R., Chuang, S., Zhang, G., and Zheng, J. (2013) Tanshinones inhibit amyloid aggregation by amyloid-β peptide, disaggregate amyloid fibrils, and protect cultured cells. *ACS Chem. Neurosci. 4*, 1004−1015.
(53) Nelson, R., Sawaya, M. R., Balbirnie, M., Madsen, A. O., Riekel, C., Grothe, R., and Eisenberg, D. (2005) Structure of the cross-beta spine of amyloid-like fibrils. *Nature 435*, 773−778.
(54) Wineman-Fisher, V., Atsmon-Raz, Y., and Miller, Y. (2015) Orientations of Residues along the β-Arch of Self-Assembled Amylin Fibril-Like Structures Lead to Polymorphism. *Biomacromolecules 16*, 156−165.
(55) Lührs, T., Ritter, C., Adrian, M., Riek-Loher, D., Bohrmann, B., Döbeli, H., Schubert, D., and Riek, R. (2005) 3D structure of Alzheimer's amyloid-β (1−42) fibrils. *Proc. Natl. Acad. Sci. U. S. A. 102*, 17342−17347.
(56) Yu, X., and Zheng, J. (2011) Polymorphic structures of Alzheimer's β-amyloid globulomers. *PLoS One 6*, e20575.
(57) Yu, X., Wang, Q., and Zheng, J. (2010) Structural determination of A[beta]25−35 micelles by molecular dynamics simulations. *Biophys. J. 99*, 666−674.
(58) Zhang, M. Z., Hu, R. D., Liang, G. Z., Chang, Y., Sun, Y., Peng, Z. M., and Zheng, J. (2014) Structural and Energetic Insight into the Cross-Seeding Amyloid Assemblies of Human IAPP and Rat IAPP. *J. Phys. Chem. B 118*, 7026−7036.
(59) Zhao, J., Yu, X., Liang, G., and Zheng, J. (2011) Structural polymorphism of human islet amyloid polypeptide (hIAPP) oligomers highlights the importance of interfacial residue interactions. *Biomacromolecules 12*, 210−220.
(60) Van der Spoel, D., Lindahl, E., Hess, B., Groenhof, G., Mark, A. E., and Berendsen, H. J. C. (2005) GROMACS: Fast, flexible, and free. *J. Comput. Chem. 26*, 1701−1718.
(61) Buck, M., Bouguet-Bonnet, S., Pastor, R. W., and MacKerell, A. D. (2006) Importance of the CMAP correction to the CHARMM22 protein force field: Dynamics of hen lysozyme. *Biophys. J. 90*, L36−L38.

DOI: 10.1021/acschemneuro.5b00192
ACS Chem. Neurosci. 2015, 6, 1759−1768